Chapter 2

2 AN OPTIMIZATION APPROACH TO THE DETERMINATION OF PLANAR MECHANISM WORKSPACES

2.1 INTRODUCTION

In this chapter an optimization approach is used to determine the workspace boundaries of two different types of planar mechanisms. The proposed optimization approach is a new and easily implemented numerical approach, which is based on a novel constrained optimization algorithm that has the considerable advantage that it may easily be automated.

The work presented here is motivated by, and stems from, the foundation paper of Haug et al. [12] which represents the state-of-the-art of computing workspaces of manipulators by the continuation method. In their paper, Haug and his co-workers emphasize the need for refined computer codes by means of which workspaces may easily be obtained.

In this chapter accessible output sets for manipulators are defined and criteria for determining their boundaries are stated. A method, based on the definition of the boundary, is developed by means of which the boundary may be mapped. In simplest terms the method consists of finding a suitable initial radiating point(s) in the output coordinate space, and then determining the points of intersection of a representative pencil of rays, which emanates from the radiating point(s), with the boundary of the accessible set. The points of intersection are determined through an optimization approach in which a proven robust dynamic constrained optimization algorithm of Snyman [37, 38] and Snyman et al. [39] is used.

The planar examples considered here are purposefully chosen to be identical to that of Haug et al. [12], so as to allow for a valid assessment of the new approach. In particular, the method is illustrated by its application to a planar Stewart platform and a planar redundantly controlled serial manipulator.

2.2 ACCESSIBLE OUTPUT SETS

In accordance with Haug et al. [12], *generalized coordinates* $\mathbf{q} = [q_1, q_2, ..., q_{nq}]^T \in R^{nq}$ are defined that characterize the position and orientation of each body in the mechanism. In the neighborhood of an *assembled configuration* of the mechanism, generalized coordinates satisfy m independent holonomic *kinematic constraint equations* of the form:

$$\Phi(\mathbf{q}) = \mathbf{0} \tag{2.1}$$

where $\Phi : R^{nq} \rightarrow R^{m}$ is a smooth function.

Mechanisms are usually designed to produce a certain functionality, where the motion of the mechanism is to be controlled by specifying the values of selected generalized coordinates, called *input coordinates*. As described by Haug et al. [12] these coordinates form a subset of the mechanism generalized coordinates, and their values are controlled by external influences with the intent of controlling the motion of the mechanism. The vector of input coordinates is denoted by $\mathbf{v} = [v_1, v_2, ..., v_{nv}]^T$.

To define the desired functionality of a mechanism, some measure of output, that is controlled by mechanism inputs, must be defined. *Output coordinates* constitute a subset of mechanism generalized coordinates that define the useful functionality of the mechanism. Output coordinates are distinct from input coordinates and are denoted by $\mathbf{u} = [u_1, u_2, ..., u_{nu}]^T$. Generalized coordinates that are neither input coordinates, nor output coordinates, are called *intermediate coordinates* denoted by $\mathbf{w} = [w_1, w_2, ..., w_{nw}]^T$, where $nw = nq - nq - nq$.

Inequality constraints are usually imposed on the input variables and often also apply to the intermediate variables. They take the form

$$\mathbf{v}^{min} \leq \mathbf{v} \leq \mathbf{v}^{max} \tag{2.2}$$

and

$$\mathbf{w}^{min} \leq \mathbf{w} \leq \mathbf{w}^{max} \tag{2.3}$$

The *accessible output set* of a manipulator is the collection of all achievable output coordinates of the manipulator. To be more precise in characterizing the accessible output set for a manipulator, the generalized coordinates are partitioned as follows:

$$\mathbf{q} = [\mathbf{u}^T, \quad \mathbf{v}^T, \quad \mathbf{w}^T]^T \tag{2.4}$$

In terms of this partition the constraint equations (2.1) may be written as:

$$\Phi(\mathbf{u},\mathbf{v},\mathbf{w}) = \mathbf{0} \tag{2.5}$$

The accessible output set A is therefore simply defined as:

$$A \equiv \{\, \mathbf{u} \in R^{nu} : \Phi(\mathbf{u},\mathbf{v},\mathbf{w}) = \mathbf{0}\,;\ \mathbf{v} \text{ satisfying (2.2) and } \mathbf{w} \text{ satisfying (2.3)} \,\} \tag{2.6}$$

Intuitively the *boundary* ∂A of the accessible output set may be defined as:

$$\partial A \equiv \{\, \mathbf{u} \in R^{nu} : \mathbf{u} \in A \ \text{ and } \exists \text{ a } \mathbf{s} \in R^{nu} \text{ such that for } \mathbf{u}' = \mathbf{u} + \lambda\mathbf{s},\ \lambda \in R$$
$$\text{arbitrary small and either positive or negative, no } \mathbf{v} \text{ and } \mathbf{w} \text{ exist that satisfy} \tag{2.7}$$
$$\Phi(\mathbf{u}', \mathbf{v}, \mathbf{w}) = \mathbf{0} \text{ as well as inequalities (2.2) and (2.3)} \,\}$$

2.3 FINDING A POINT ON ∂A

A distinction is made with respect to system of equations (2.1) and (2.5), between two possibilities:

Case (i): where $m = nv$ and, given **u** and **w**, system (2.5) may easily be solved to give **v** in terms of **u** and **w**:

$$\mathbf{v} = \mathbf{v}(\mathbf{u},\mathbf{w}) \tag{2.8}$$

This is typically the situation with parallel manipulators where the inverse kinematics is easy to solve.

Case (ii): where $m = nu$ and, given **v** and **w**, system (2.5) may easily be solved to give **u** in terms of **v** and **w**:

$$\mathbf{u} = \mathbf{u}(\mathbf{v},\mathbf{w}) \tag{2.9}$$

This again is typical for serially linked manipulators where the forward kinematics is relatively easy to solve.

First consider first *Case (i)*. Assume that a radiating point $\mathbf{u}^0$ of A is available, and for the moment assume that it is interior to the accessible set. It is now proposed that, consistent with the definition of ∂A in (2.7), a point $\mathbf{u}^b$ on the boundary in the direction $\mathbf{s} \in R^{nu}$ from $\mathbf{u}^0$ be determined by solving the following constrained optimization problem:

Problem (i):

$$\underset{\mathbf{u},\mathbf{w}}{\textit{maximize}} \quad \left\|\mathbf{u}-\mathbf{u}^0\right\|$$

$$\textit{such that:} \quad \begin{aligned} \mathbf{v}^{\min} &\le \mathbf{v}(\mathbf{u},\mathbf{w}) \le \mathbf{v}^{\max} \\ \mathbf{w}^{\min} &\le \mathbf{w} \le \mathbf{w}^{\max} \end{aligned}$$

$$\textit{and subject to equality constraints:} \quad \mathbf{h}(\mathbf{u},\mathbf{s})=\mathbf{0},\ \mathbf{h}\in \mathrm{R}^{nu-1}$$

which defines a point on the parameterized straight line ray, $\mathbf{u}(\lambda)=\mathbf{u}^0+\lambda\mathbf{s},\ \lambda\in\mathrm{R}$. Here $\|\cdot\|$ denotes the Euclidean norm. {For example, if $nu=2$, $\mathbf{u}=[x,y]^{\mathrm{T}}$, $\mathbf{u}^0=[x^0,y^0]^{\mathrm{T}}$, and $\mathbf{s}=[\mathrm{s}_x,\mathrm{s}_y]^{\mathrm{T}}$, then $\mathbf{u}=\mathbf{u}^0+\lambda\mathbf{s}$ has the components $x=x^0+\lambda\mathrm{s}_x$; $y=y^0+\lambda\mathrm{s}_y$ and it follows that: $\mathrm{h}(\mathbf{u},\mathbf{s})=(x-x^0)/\mathrm{s}_x-(y-y^0)/\mathrm{s}_y=0$ } (see Figure 2.1)

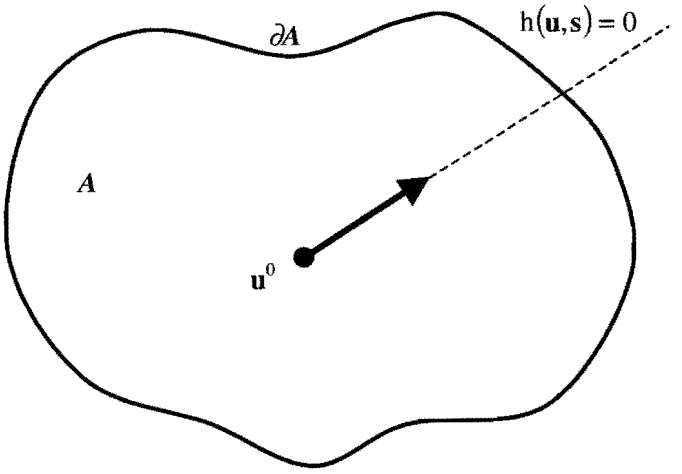

Figure 2.1 Ray in A from $\mathbf{u}^0$ to ∂A.

For *Case (ii)* the associated constrained optimization problem is given by:

Problem (ii):

$$\underset{\mathbf{v},\mathbf{w}}{\textit{maximize}} \quad \left\|\mathbf{u}(\mathbf{v},\mathbf{w})-\mathbf{u}^0\right\|$$

$$\textit{such that:} \quad \begin{aligned} \mathbf{v}^{\min} &\le \mathbf{v} \le \mathbf{v}^{\max} \\ \mathbf{w}^{\min} &\le \mathbf{w} \le \mathbf{w}^{\max} \end{aligned}$$

$$\textit{and subject to equality constraints:} \quad \mathbf{h}(\mathbf{u}(\mathbf{v},\mathbf{w}),\mathbf{s})=\mathbf{0}$$

where the equality constraint defines a point $\mathbf{u}$ on the straight line through $\mathbf{u}^0$ in the direction $\mathbf{s}$.

Note that should $\mathbf{u}^0$ be chosen to be exterior to A, then the optimization problems above obviously become *minimization* problems.

In this chapter, the presentation will be restricted to planar mechanisms. In Chapter 3 the methodology developed here for and applied to planar mechanisms, will be extended to spatial mechanisms.

2.4 BASIC METHODOLOGY FOR MAPPING THE BOUNDARY OF A PLANAR ACCESSIBLE SET

Assume a planar manipulator with a two-dimensional accessible set $\boldsymbol{A}$, and also for the moment assume that $\boldsymbol{A}$ is convex, which certainly will not always be the case. Also assume, for the moment, that the radiating point $\mathbf{u}^0$ is an interior point as shown in Figure 2.2.

The boundary $\partial \boldsymbol{A}$ may now be numerically mapped by solving the appropriate optimization problem ((i) or (ii)) for N successive rays, with respective directions $\mathbf{s}^i, i = 0,1,2,...,N$, emanating at angular intervals of δ (where for example $\delta = 360^\circ/N$) from $\mathbf{u}^0 = [x^0, y^0]^T$ as depicted in Figure 2.2.

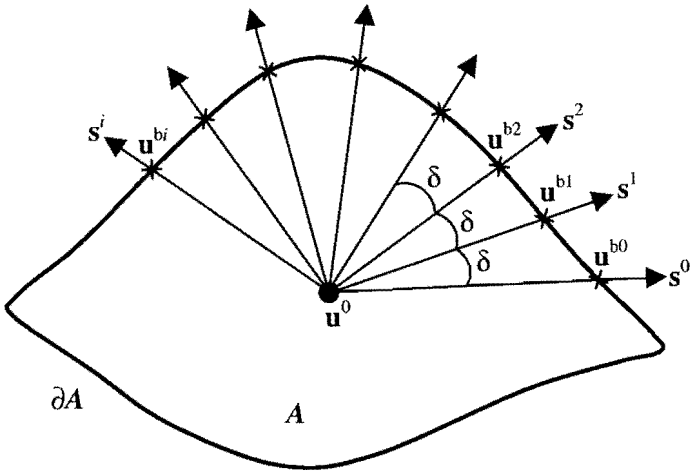

Figure 2.2 Numerical map of $\partial \boldsymbol{A}$; $\mathbf{u}^{bi}$, $i = 0,1,...,N$.

Questions now arise in connection with details of the implementation of the methodology. The first question relates to how an *initial* radiating point $\mathbf{u}^0$ may be obtained. Depending on the particular geometry of each case, a suitable choice for $\mathbf{u}^0$ may be self-evident. If not, it is suggested that, in *Case (i)*, $\mathbf{u}^0$ may be obtained from equation (2.8) by solving for $\mathbf{u}$ in:

$$\overline{\mathbf{v}} = \mathbf{v}(\mathbf{u}, \overline{\mathbf{w}}) \qquad (2.10)$$

where

$$\overline{\mathbf{v}} = \left(\mathbf{v}^{\min} + \mathbf{v}^{\max}\right)/2$$
$$\overline{\mathbf{w}} = \left(\mathbf{w}^{\min} + \mathbf{w}^{\max}\right)/2$$

In practice this may be done by solving the least squares optimization problem

$$\underset{\mathbf{u}}{minimize} \ \left\|\mathbf{v}(\mathbf{u}, \overline{\mathbf{w}}) - \overline{\mathbf{v}}\right\|^2 \qquad (2.11)$$

In *Case (ii)*, if an obvious choice for $\mathbf{u}^0$ is not available, then an indication may be obtained from equation (2.9):

$$\mathbf{u}^0 = \mathbf{u}(\overline{\mathbf{v}}, \overline{\mathbf{w}}) \tag{2.12}$$

The second question concerns the strategy to be adopted if non-convexity of $\boldsymbol{A}$ interferes with the mapping as illustrated in Figure 2.3, where as result of the non-convexity, two boundary points $\mathbf{u}_1^b$ and $\mathbf{u}_2^b$ exist.

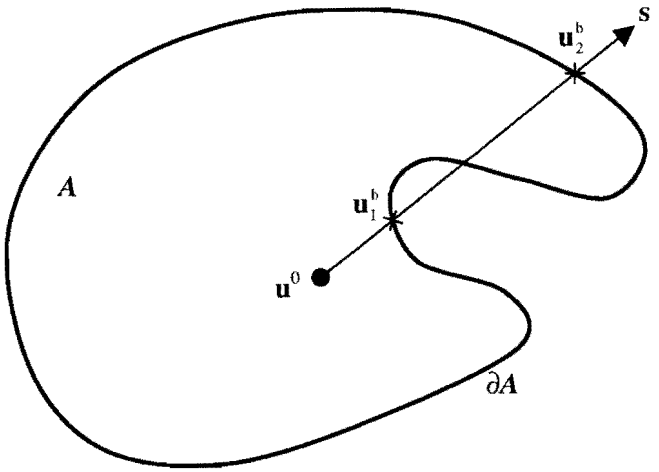

Figure 2.3 Complication if $\boldsymbol{A}$ is non-convex.

If this happens, it will be necessary to adjust $\mathbf{u}^0$ such that the boundary point $\mathbf{u}^b$ is unique for a prescribed search direction $\mathbf{s}$. The precise strategy to be adopted will be described separately in the later sections dealing with the application of the methodology. A final question that must be addressed, is what procedure to adopt if the boundary mapping approaches a bifurcation point. The procedure to deal with such an eventuality is also described in the sections dealing with the applications.

2.5 APPLICATION TO THE PLANAR SERIAL MANIPULATOR

Although the emphasis of this study is on determining the workspaces of parallel manipulators, the versatility of the optimization method should at least correspond to that of Haug et al's [12] continuation method. Consequently, the serial manipulator studied by Haug et al. [12] is also investigated in this section using the optimization approach.

2.5.1 Geometry of the Planar Serial Manipulator

The redundantly controlled serial manipulator shown in Figure 2.4 was therefore purposefully taken from Haug et al. [12]. This is a planar manipulator with three links, and three revolute joints.

Revolute joint 1 is the connection between the serial manipulator and the ground. The global coordinate system is fixed with the origin coinciding with joint 1. The orientation angle of link 1 relative to the

positive X-axis, is indicated by θ_1, and is measured in a right hand sense about the origin of the fixed global coordinate system. Similarly θ_2 and θ_3 measures the orientation angles of respectively link 2 with link 1, and link 3 with link 2. Depending on the configuration of the serial manipulator, the orientation angles can be positive, or negative.

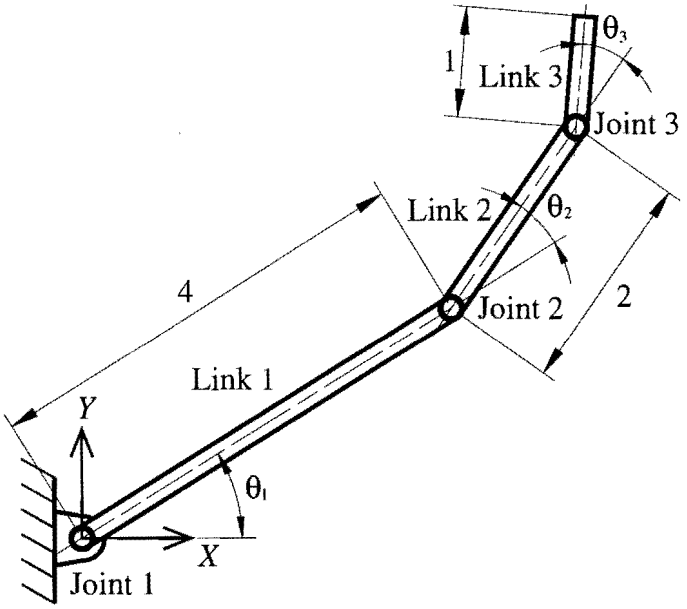

Figure 2.4 Planar serial manipulator with redundant input.

The working point P is the end point of link 3, which is the position where in practice some end effector is mounted. The accessible region of the working point depends on the upper and lower orientation angle limitations. In accordance to Haug et al. [12], the same limitations are imposed on all three orientation angles. Expressing the constraint equations in terms of the orientation angles in radians, gives:

$$-\frac{\pi}{3} = \theta_i^{\min} \le \theta_i \le \theta_i^{\max} = \frac{\pi}{3} \tag{2.13}$$

This choice of angle limits clearly causes the workspace to be symmetric about the positive X-axis, and one also intuitively expects the workspace to be non-convex.

2.5.2 Constraint Equations of the Planar Serial Manipulator

With reference to Section 2.2 , equation (2.13) is the serial manipulator version of the general inequality constraints (2.2). Here the orientation angles are obviously the *input variables*, i.e. $\mathbf{v} = [\theta_1, \theta_2, \theta_3]^T$, and the global coordinates of the working point P are the *output coordinates*, i.e. $\mathbf{u} = [x, y]^T$. There are no *intermediate coordinates* required in describing the serial manipulator.

The serial manipulator therefore has five generalized coordinates (2.4):

$$\mathbf{q} = \left[\mathbf{u}^T, \mathbf{v}^T\right]^T = \left[x, y, \theta_1, \theta_2, \theta_3\right]^T$$

Having only two degrees of freedom, and three inputs, makes the serial manipulator redundantly controlled. This means that the same output coordinates can be obtained with different sets of input coordinates. The situation becomes clearer when looking at the two kinematic constraint equations corresponding to general form (2.5). Doing the forward kinematic analysis for the serial manipulator, gives expressions for the output coordinates in terms of the input angles ($\theta_i, i = 1, 2, 3$):

$$\begin{aligned} x &= 4\cos\theta_1 + 2\cos(\theta_1 + \theta_2) + \cos(\theta_1 + \theta_2 + \theta_3) \\ y &= 4\sin\theta_1 + 2\sin(\theta_1 + \theta_2) + \sin(\theta_1 + \theta_2 + \theta_3) \end{aligned} \tag{2.14}$$

Having two equations in three variables results in the existence of multiple solutions for a particular choice of (x, y).

Rewriting equation (2.14) in the general form (2.5), gives:

$$\mathbf{\Phi}(\mathbf{u}, \mathbf{v}) = \begin{bmatrix} u_1 - 4\cos(v_1) - 2\cos(v_1 + v_2) - \cos(v_1 + v_2 + v_3) \\ u_2 - 4\sin(v_1) - 2\sin(v_1 + v_2) - \sin(v_1 + v_2 + v_3) \end{bmatrix} = \mathbf{0} \tag{2.15}$$

from which explicit expressions for $\mathbf{u}$ follows:

$$\mathbf{u}(\mathbf{v}) = \begin{bmatrix} 4\cos(v_1) + 2\cos(v_1 + v_2) + \cos(v_1 + v_2 + v_3) \\ 4\sin(v_1) + 2\sin(v_1 + v_2) + \sin(v_1 + v_2 + v_3) \end{bmatrix} \tag{2.16}$$

The inequality constraints given by expression (2.13) can be written in the standard form (2.2):

$$\begin{gathered} \mathbf{v}^{min} \le \mathbf{v} \le \mathbf{v}^{max} \\ \text{where } \mathbf{v}^{min} = \left[\theta_1^{min}, \theta_2^{min}, \theta_3^{min}\right]^T \text{ and } \mathbf{v}^{max} = \left[\theta_1^{max}, \theta_2^{max}, \theta_3^{max}\right]^T \end{gathered} \tag{2.17}$$

Notice that the serial manipulator can be classified under *Case (ii)* of Section 2.3. Expressions (2.17), (2.16) and (2.15) which were specifically derived for the serial manipulator, correspond to the general expressions (2.2), (2.9) and (2.5). The boundary ∂A of the accessible set of the serial manipulator may therefore be numerically determined by applying the basic methodology described in Section 2.4 and in which optimization *Problem (ii)* of Section 2.3 is successively solved.

The specific constrained optimization method used in solving the optimization problems is the dynamic trajectory method of Snyman [37], [38] for unconstrained optimization, applied to penalty function formulations (Snyman et al. [39], Snyman [40]) of the constrained problems. The particular computer code used is *LFOPCV3* (Snyman [40]).

2.5.3 Discussion of Results for the Planar Serial Manipulator

2.5.3.1 Outer Accessible Workspace Boundary

Figure 2.5 shows the outer accessible workspace boundary obtained.

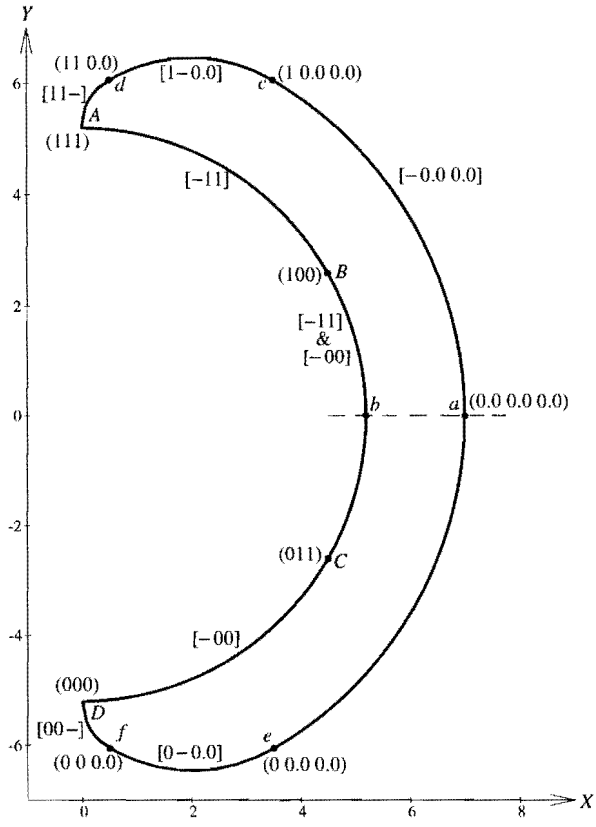

Figure 2.5 Boundary of the accessible output set of the planar serial manipulator.

With the workspace being symmetrical about the positive X-axis, only the top half is computed. The radiating point for determining the workspace is chosen to be at the origin of the global coordinate system, i.e. $\mathbf{u}^0 = [0, 0]^T$. This choice for the radiating point allows for the separation of the outer workspace boundary into a far and a near boundary.

Looking at only the top half of the accessible output set, it is clear that the near and far boundaries are smooth curves, which meet at an *extreme point A*. The working point of the serial manipulator will be at this extreme point A, if the input angles take on their respective maximum values, i.e. $\mathbf{v}_i = \mathbf{v}_i^{\max}$ for $i = 1, 2, 3$. The output coordinates of point A are determined by substituting these maximum values of $\mathbf{v}_i$ in equation (2.16), resulting in $\mathbf{u}^A = [0.0,\ 5.1962]^T$.

For the top half, the outer boundary is mapped by successively solving optimization *Problem (ii)* for successive rays emanating from the radiating point $\mathbf{u}_0$ which, for the far boundary, is effectively an

interior point. The *maximization* is carried out for successive search directions $\mathbf{s}_i, i = 1, 2, ..., N$, each corresponding to a radiating angle ψ_i. Here $\psi_1 = 0$ and $\psi_N = \pi/2$, with the other angles suitably and monotonically spaced in between. Clearly $\psi_N = \pi/2$ corresponds to the ray passing through $\mathbf{u}^A$.

As soon as the point *A* is reached, *Problem (ii)* becomes a *minimization* problem since, for the mapping of the near boundary, $\mathbf{u}^0$ is now an exterior point. The inner boundary is now mapped by successively carrying out the minimization, but now for successive angles decreasing from $\psi_{1'} = \pi/2$ and $\psi_{N'} = 0$. The bottom half of the workspace boundary is simply a mirror image of the top half.

In the mapping, depending on the curvature of the workspace boundary, provision is made for adjusting the angular interval between rays so as to ensure sufficient accuracy.

Haug et al. [12] not only manage to determine the accessible workspace boundaries of the serial manipulator, they also describe the behavior of the manipulator associated with different curves of the workspace. Their method enables them to find the bifurcation points located within, and on the boundaries of the accessible output set. These bifurcation points are numbered, and each curve connecting two bifurcation points is "described" with reference to those input variables that remain fixed, and those input variables that vary as the manipulator advances along the specific curve.

Here, an alternative and more concise notation for labeling the bifurcation points and boundary curves is proposed. This should facilitate the discussion of the results.

The serial manipulator working point *P* will coincide with a bifurcation point if all the input angles are fixed at (usually) either their maximum or minimum allowable values. If for each input angle ($\theta_i, i = 1, 2, 3$), the state is indicated by setting $X_i := 0$ for the minimum allowable value and $X_i := 1$ for the maximum allowable value, then the configuration of the manipulator at a specific bifurcation point may be indicated and labeled by a triplet enclosed in round brackets, $(X_1\ X_2\ X_3)$. Thus point *A* in Figure 2.5 where all three input angles have maximum values is, for example, labeled by $(1\ 1\ 1)$.

The boundary curves may be labeled in a similar manner. Usually, as one moves from one bifurcation point to the next along a particular boundary curve, the value of one of the input angles, say *j*, varies from one extreme bound to the other. This may be indicated by setting $X_j := -$ and $X_i := 0$ or 1 for $i \neq j$, depending on whether input angle *i* assumes a minimum or maximum value. The curve may therefore be labeled by a triplet enclosed in square brackets, $[X_1\ X_2\ X_3]$.

On closer inspection of the results for the far boundary *aA* in Figure 2.5, three distinct curves are identified. Along curve *ac* the serial manipulator is stretched and the three links form a straight line. The working point will advance along this curve as it moves on an arc of radius $= 4+2+1=7$, with center of radius at the origin of the global coordinate system.

The proposed notation for labeling the boundary curves and bifurcation points is slightly modified to accommodate curves and points where the input variables take on fixed values other than the extreme values corresponding to bounds.

Curve ce is labeled [– 0.0 0.0] indicating that input variable v_1 varies between its minimum and maximum values, while input variables v_2 and v_3 both remain fixed at 0.0. The top half of curve *ce* [– 0.0 0.0] is curve *ac*, where input variable v_1 varies between zero and its maximum value. Point *c* is labeled as (1 0.0 0.0) indicating that $\mathbf{v}^c = [v_1^{max}, 0.0, 0.0]^T$ while point *a* is labeled (0.0 0.0 0.0) indicating that $\mathbf{v}^a = [0.0, 0.0, 0.0]^T$. The global coordinates of point *c* are $\mathbf{u}^c = [3.5,\ 6.0622]^T$. The bottom half of curve *ce* [– 0.0 0.0] is curve *ae* where input variable v_1 varies between zero and its minimum value, while v_2 and v_3 remain fixed at 0.0. Point *e* is labeled (0 0.0 0.0) indicating that $\mathbf{v}^e = [v_1^{min}, 0.0, 0.0]^T$, and the global coordinates of point *e* are $\mathbf{u}^e = [3.5,\ -6.0622]^T$

With v_1 fixed at $v_1^{max} = \pi/3$, the working point will map the curve *cd* [1 – 0.0] as it moves on an arc of radius $= 2+1=3$ with the center of radius coinciding with the position of revolute joint 2. The mirror image of curve *cd* [1 – 0.0] is curve *ef* [0 – 0.0], where v_1 is fixed at $v_1^{min} = -\pi/3$. Finally with input variables v_1 and v_2 both fixed at their maximum values, curve *dA* [1 1 –] lies on an arc of radius $= 1$, with center of radius situated at revolute joint 3. It follows that the mirror image of curve *dA* [1 1 –] is curve *fD* [0 0 –], where input variables v_1 and v_2 both fixed at their minimum values.

The inner boundary of the workspace is an arc of radius $= 5.1962$ which joins bifurcation points *A* and *D*. The arc radius is the shortest possible distance from the global coordinate system origin to the working point, and can be obtained with both input variables v_2 and v_3 either at their maximum, or minimum values. Curve *AD* in fact consist of two overlapping bifurcation curves *AC* [– 1 1], and *BD* [– 0 0]. The global coordinates of any bifurcation point can easily be determined from equation (2.16).

Clearly in this specific case, the near boundary could have been obtained by a simple and obvious geometrical construction, rather than by the general optimization mapping used here.

2.5.3.2 Curves Connecting Bifurcation Points

For the serial manipulator under consideration, four bifurcation points are situated inside the workspace boundaries, namely points *E*, *F*, *G* and *H* as shown in Figure 2.6.

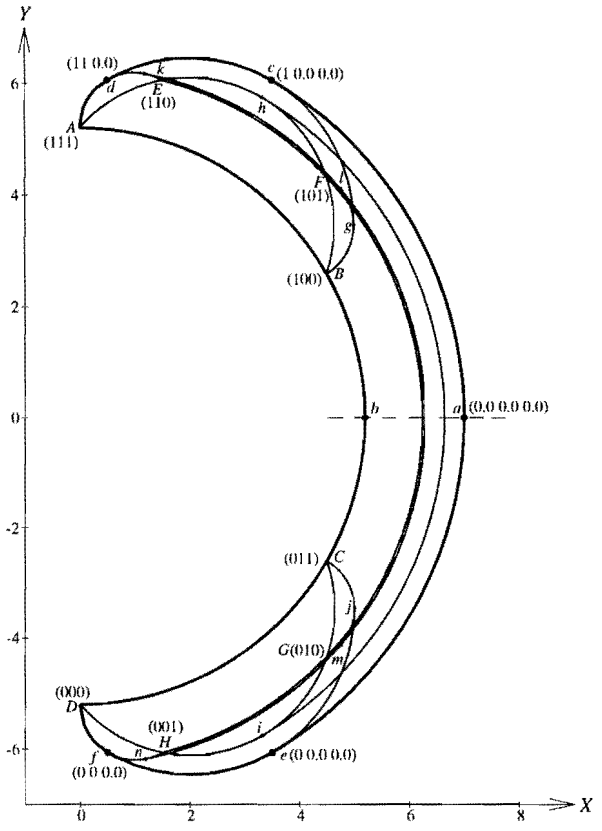

Figure 2.6 Interior bifurcation points and curves of the planar serial manipulator.

Figure 2.6 also shows interior curves connecting these bifurcation points. For clarity, a magnified view of the upper segments is shown in Figure 2.7. The interior curves connecting the bifurcation points, are mapped using forward kinematic analyses. Taking curve AdE $[1\ 1\ -]$ as an example: M points along curve AdE $[1\ 1\ -]$ can easily be mapped by setting $v_1 = v_1^{max}$, $v_2 = v_2^{max}$ and $v_3 = v_3^j$, where

$$v_3^j = v_3^{max} - \frac{j}{M}\left(v_3^{max} - v_3^{min}\right)$$

and solving for each setting j, $j = 0, 1, 2, \ldots, M$ equation (2.16) directly to give the corresponding output coordinates $\mathbf{u}(\mathbf{v})$.

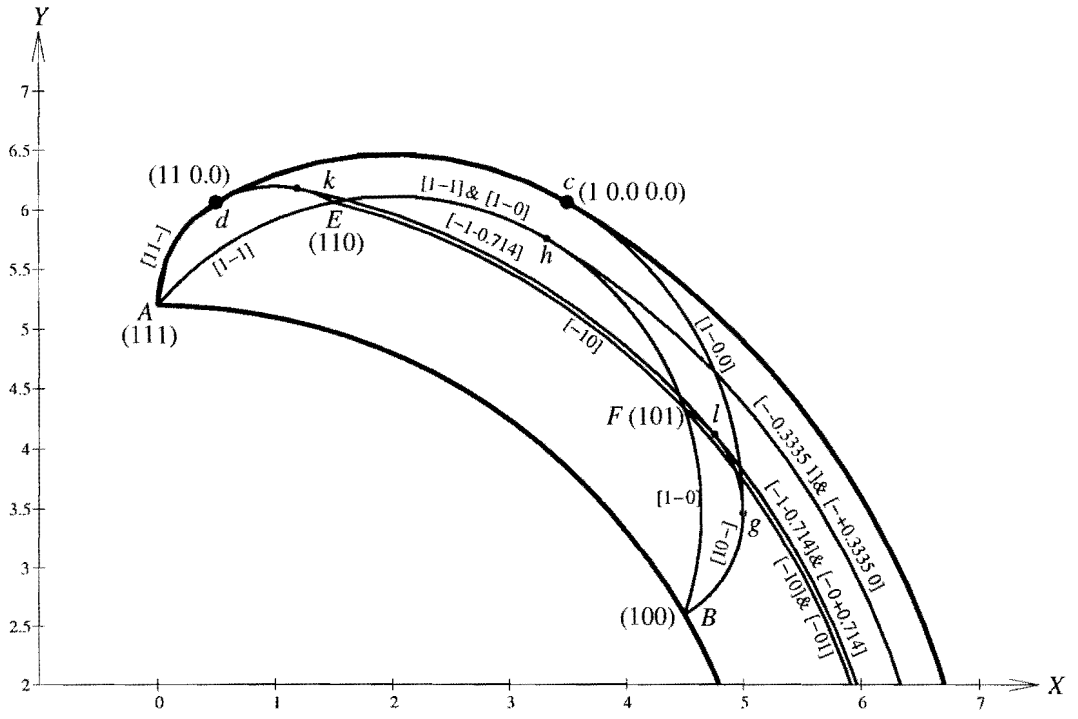

Figure 2.7 Magnified view of upper part of boundary and bifurcation curves of planar serial manipulator.

Curve *cg* $[1\ -\ 0.0]$ does not connect any bifurcation points, but is the interior extension of the second arc *de* on the far boundary described in Section 2.5.3.1. The mapping of this curve is done in a similar manner to that described for curve *AE* above. Curve *ej* $[0\ -\ 0.0]$ is the mirror image of curve *cg* $[1\ -\ 0.0]$.

The final two interior paths to be dealt with, are path *hi* and path *klmn* also reported by Haug et al. [12]. Path *hi* lies on an arc with radius $= 6.64575$, and center point at $(0.0,\ 0.0)$. The radius is obtained by solving optimization *Problem (ii)* with $-\pi/3 = v_i^{min} \le v_i \le v_i^{max} = \pi/3$ for $i = 1$ and 2, and $v_3 = v_3^{max} = \pi/3$.

Here it was noticed that with variation in the search direction, v_1 varies, but v_2 remains constant at the value $v_2 = -0.3335$. If v_3 is fixed at $v_3 = v_3^{max} = \pi/3$, then carrying out the optimization for different search directions, v_1 varies again but v_2 takes on the constant value $v_2 = +0.3335$. The respective computed curves *hi* $[-\ -0.3335\ \ 1]$ and *ih* $[-\ +0.3335\ \ 1]$ coincide as shown.

Path *klmn* is computed similarly and lies on an arc of radius 6.2915. This curve consists of two partially overlapping curves *km* $[-\ \ 1\ \ -0.714]$, and *ln* $[-\ \ 1\ \ +0.714]$ as shown in Figure 2.6.

It should be stated that the respective constant values (0.3335 and 0.714) assumed by v_2 for the curves *ih* and *ln* differ slightly from that (0.3241 and 0.7499) reported by Haug et al. [12].

2.6 APPLICATION TO THE PLANAR STEWART PLATFORM

In the remaining part of this study, the emphasis falls on Stewart platform workspaces, and specifically how the optimization approach is utilized in analyzing and characterizing the different workspaces. This section deals with determining the exterior boundaries of the accessible workspace of a planar Stewart platform, as well as finding the bifurcation point connecting curves.

2.6.1 Geometry of the Planar Stewart Platform

The geometry of the planar Stewart platform considered here is taken from Haug et al. [12], and is as shown in Figure 2.8.

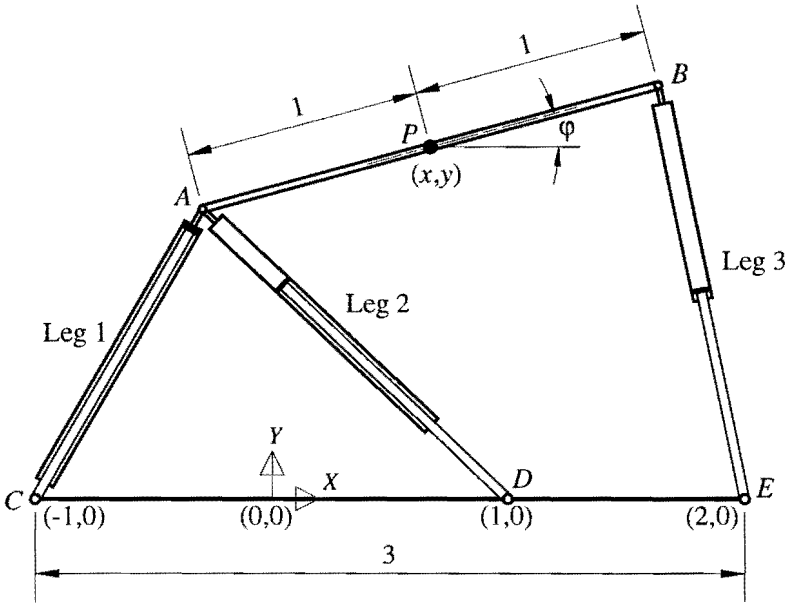

Figure 2.8 Planar Stewart platform.

The moving upper platform is connected to the fixed base via three linear actuators such as, for example, hydraulic cylinders. The base can in general be fixed in any orientation but in this case it is fixed horizontally. The global coordinate system was chosen to be on the base, with the origin midway between joints *C* and *D*, and with the directions of the axes as shown in Figure 2.8.

The lower ends of the actuator legs are connected to the base at points *C*, *D* and *E* with respective global coordinates $(-1,0)$, $(1,0)$ and $(2,0)$. The upper ends of actuator legs 1 and 2 are both connected to the left hand side of the top platform at point *A*. Actuator leg 3 has its upper end connected to the right side

of the top platform at B. The working point P is at the center of the top platform at global position (x, y) with the platform making an angle φ with the horizontal.

Each of the three actuator legs is a variable length linear actuator with its length indicated by l_i, $i = 1, 2, 3$. There are limitations on the maximum and minimum lengths of linear actuators, and therefore the accessible region of the working point P is determined by the constraints on the actuator lengths which are formally expressed as:

$$0 < l_i^{\min} \leq l_i < l_i^{\max} \tag{2.18}$$

for $i = 1, 2, 3$

The actual leg length limits that are used, are the same as the limits specified by Haug et al. [12], and are given in Table 2.1.

Leg i	$l_i^{\min}$	$l_i^{\max}$
1	$\sqrt{2}$	2
2	$\sqrt{2}$	2
3	1	$\sqrt{3}$

Table 2.1 Minimum- and maximum lengths of the actuator legs.

2.6.2 Constraint Equations of the Planar Stewart Platform

Clearly for the planar Stewart platform, and with reference to the definitions given in Section 2.2, the actuator leg lengths are the *input variables*, i.e. $\mathbf{v} = [l_1, l_2, l_3]^T$, on which the inequality constraints (2.18) are imposed corresponding to the general constraints (2.2). The global coordinates of the working point are the *output variables*, i.e. $\mathbf{u} = [x, y]^T$. The rotation angle φ of the top platform is the one and only *intermediate coordinate*, i.e. $\mathrm{w} = \varphi$. Here, no inequality constraints of the general form (2.3), are imposed on the intermediate variable w.

The generalized coordinates (2.4) for the Stewart platform are given by

$$\begin{aligned} \mathbf{q} &= \begin{bmatrix} \mathbf{u}^T & \mathbf{v}^T & \mathbf{w}^T \end{bmatrix}^T \\ &= \begin{bmatrix} \mathbf{u}^T & \mathbf{v}^T & \mathrm{w} \end{bmatrix}^T \\ &= [x,\ y,\ l_1,\ l_2,\ l_3,\ \varphi]^T \end{aligned} \tag{2.19}$$

This system clearly has three degrees of freedom, since the configuration of the system is uniquely defined by any three of these coordinates. This implies the existence of three kinematic constraint equations of the form (2.5), specifying the interrelationships between the coordinates.

From the geometry shown in Figure 2.8, the inverse kinematics may easily be performed to give the actuator lengths in terms of x, y and φ:

$$\begin{aligned} l_1^2 &= (x - \cos\varphi + 1)^2 + (y - \sin\varphi)^2 \\ l_2^2 &= (1 - x + \cos\varphi)^2 + (y - \sin\varphi)^2 \\ l_3^2 &= (x + \cos\varphi - 2)^2 + (y - \sin\varphi)^2 \end{aligned} \tag{2.20}$$

The above may be rewritten in the standard form (2.5) for the constraint equations as:

$$\mathbf{\Phi}(\mathbf{u},\ \mathbf{v},\ \mathrm{w}) = \begin{bmatrix} \mathrm{v}_1^2 - (\mathrm{u}_1 - \cos(\mathrm{w}) + 1)^2 - (\mathrm{u}_2 - \sin(\mathrm{w}))^2 \\ \mathrm{v}_2^2 - (1 - \mathrm{u}_1 + \cos(\mathrm{w}))^2 - (\mathrm{u}_2 - \sin(\mathrm{w}))^2 \\ \mathrm{v}_3^2 - (\mathrm{u}_1 + \cos(\mathrm{w}) - 2)^2 - (\mathrm{u}_2 - \sin(\mathrm{w}))^2 \end{bmatrix} = \mathbf{0} \tag{2.21}$$

from which the explicit expressions for $\mathbf{v}$ follow:

$$\mathbf{v} = \mathbf{v}(\mathbf{u}, \mathrm{w}) = \begin{bmatrix} \sqrt{(\mathrm{u}_1 - \cos(\mathrm{w}) + 1)^2 + (\mathrm{u}_2 - \sin(\mathrm{w}))^2} \\ \sqrt{(1 - \mathrm{u}_1 + \cos(\mathrm{w}))^2 + (\mathrm{u}_2 - \sin(\mathrm{w}))^2} \\ \sqrt{(\mathrm{u}_1 + \cos(\mathrm{w}) - 2)^2 + (\mathrm{u}_2 - \sin(\mathrm{w}))^2} \end{bmatrix} \tag{2.22}$$

Inequalities (2.18) may also be written in the standard form:

$$\begin{gathered} \mathbf{v}^{\min} \le \mathbf{v} \le \mathbf{v}^{\max} \\ \text{where } \mathbf{v}^{\min} = \left[l_1^{\min}, l_2^{\min}, l_3^{\min}\right]^{\mathrm{T}} \text{ and } \mathbf{v}^{\max} = \left[l_1^{\max}, l_2^{\max}, l_3^{\max}\right]^{\mathrm{T}} \\ \text{and } \mathbf{v} = \mathbf{v}(\mathbf{u}, \mathrm{w}) \text{ as given by (2.22)} \end{gathered} \tag{2.23}$$

Now expressions (2.23), (2.21) and (2.22) for the planar Stewart platform, clearly correspond to *Case (i)* of Section 2.3 , specified in general by expressions (2.2), (2.5) and (2.8).

The method used to determine the boundary ∂A of the accessible output set for the planar Stewart platform is similar to the method used for the serial manipulator. The only difference is that for the planar Stewart platform optimization *Problem (i)* is successively solved. The computer code *LFOPCV3* [40] is again used to solve the optimization problems.

Note that here there is no explicit restriction (2.3) on w. This implies that there are no limitations on the orientation angle of the top platform, therefore the workspace boundary is solely dependant on the limitations imposed on the actuator leg lengths. This is called the *accessible* or *reachable workspace* defined by Kumar [11] as the "volume or space within which a reference point on the hand or end effector of a manipulator can be made to coincide with any point in the volume or space".

2.6.3 Discussion of Accessible Workspace Results for the Planar Stewart Platform

2.6.3.1 Outer Accessible Workspace Boundary

The computed outer boundaries of the accessible workspaces for two different situations are shown in Figure 2.9 and Figure 2.10. For the cases depicted here, the *boundary mapping* was done at intervals of $\delta = 5^\circ$ (see Figure 2.2).

Figure 2.9 shows the boundary of the accessible output set of the *standard* planar Stewart platform for which the limits on the actuator lengths, given in Table 2.1, are such as to prevent a singular configuration from occurring. Such a singularity will occur if the upper platform is allowed to take on a position that is collinear with any of the actuators (Haug et al. [41]).

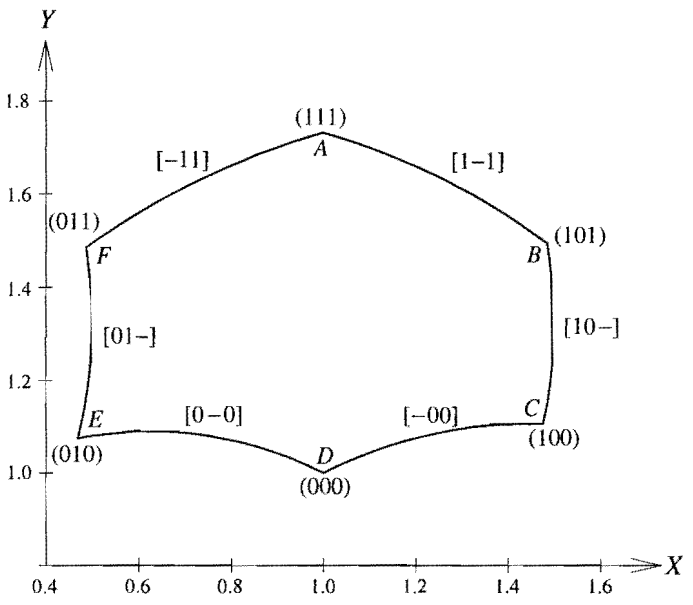

Figure 2.9 Boundary of the accessible output set of the *standard* planar Stewart platform $(1 \le l_3 \le \sqrt{3})$.

The methodology described in Section 2.4, represented by the least squares problem (2.11), is used to find the central radiating point for the planar Stewart platform. The central point for the *standard* planar Stewart platform is $\mathbf{u}^0 = [0.99996 \quad 1.374791]^T$.

Figure 2.10 shows the results for the *modified* planar Stewart platform, where the limitations on actuator leg 3 is relaxed to $1 \le l_3 \le 3$. This was also done by Haug et al. [12] to allow for collinearity to occur. The central radiating point for this second situation is $\mathbf{u}^0 = [0.95169 \quad 1.69061]^T$.

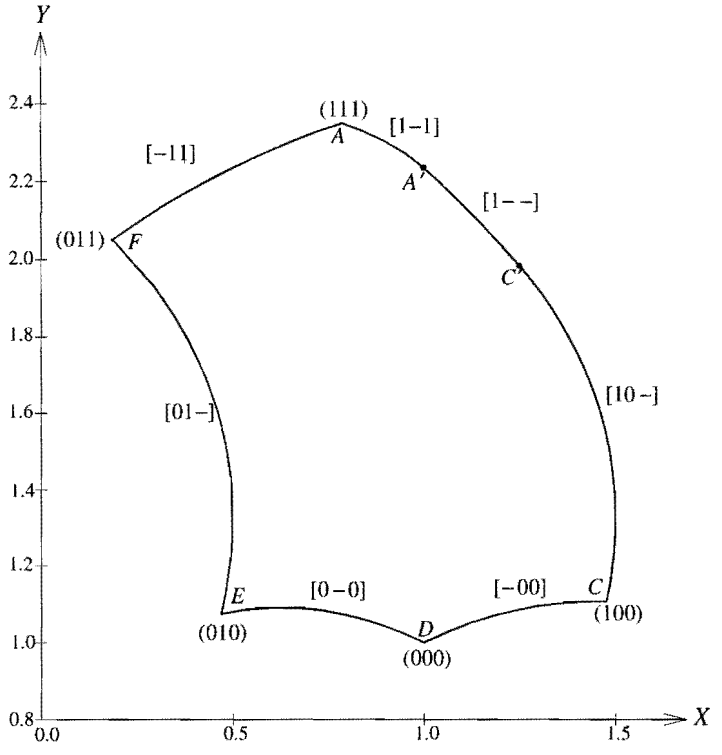

Figure 2.10 Boundary of the accessible output set of the *modified* planar Stewart platform ($1 \le l_3 \le 3$).

One notices that the boundary of the workspace for the standard case is defined by six smooth curves intersecting at distinct corners *A*, *B*, *C*, *D*, *E* and *F*. On closer inspection of the results, it becomes clear that one may easily relate the various curves of the workspace boundary to the behavior of the Stewart platform. This was indeed done by Haug et al. [12] in identifying the corners as bifurcation points and numbering them. The individual boundary curves were then labeled according to the numbers of the bifurcation points they connected and the variation of the actuator lengths were tabulated for each curve.

With reference to Section 2.5.3.1 the newly proposed notations for labeling the bifurcation points and boundary curves are also applied here to describe the workspace of the planar Stewart platform. Labeling the bifurcation points in the proposed manner indicates which actuator legs are at their minimum values, and which assume their maximum lengths when the manipulator working point coincides with any specific bifurcation point. Thus point *A* in Figure 2.9 and Figure 2.10, where all three legs have maximum values is, labeled by $(1\ 1\ 1)$. The other boundary bifurcation points of the standard planar Stewart platform are similarly labeled as shown in Figure 2.9.

Similarly, the square bracket triplets with which the boundary curves are labeled, indicate which legs remain fixed at either their minimum or maximum bounds, and which legs vary from one extreme to the other as the manipulator working point moves from one extreme to the other. Consider, as an example, boundary curve AB connecting bifurcation point A $(1\ 1\ 1)$ to bifurcation point B $(1\ 0\ 1)$ in Figure 2.9. This curve is labeled by $[1\ -\ 1]$, indicating that legs 1 and 3 remain fixed at their respective maximum lengths, and leg 2 varies from its maximum length (working point coinciding with A) to its minimum length (working point coinciding with B). The other boundary curves are labeled in a similar manner.

The precise mapping of the bifurcation point corners is done by, having identified through the boundary mapping procedure the three active constraints at the corner, then minimizing $\left\|\mathbf{v}(\mathbf{u}, w) - \mathbf{v}^a\right\|^2$ with respect to $\mathbf{u}$ and w, where $\mathbf{v}^a$ corresponds to the leg lengths associated with the three identified equality constraints. This bifurcation point mapping is automatically done by the computer code as it maps the boundary.

The results for the modified planar Stewart platform is qualitatively the same as for the standard platform, except that for the modified case there is only five smooth boundary curves with bifurcation point B $(1\ 0\ 1)$ lying inside the workspace. Here the two smooth boundary curves AB and BC of the standard case blend into a single smooth boundary curve AC, which consists of three parts: AA' $[1\ -\ 1]$, $A'C'$ $[1\ -\ -]$, and $C'C$ $[1\ 0\ -]$. It is clear that along $A'C'$ the platform is stretched to be collinear with actuator leg 1 so that only the single constraint $l_1 = l_1^{max}$ is active.

The point A' may be determined in a manner similar to the way in which the corner bifurcation points were obtained by minimizing, with regard to $\mathbf{u}$ and $\mathbf{v}$, the following error function:

$$e(\mathbf{u}, w) = \left(v_1(\mathbf{u}, w) - v_1^{max}\right)^2 + \left(v_3(\mathbf{u}, w) - v_3^{max}\right)^2 + \left(u_2 - (u_1 + 1)\tan(w)\right)^2 \qquad (2.24)$$

The first two terms of error function (2.24) correspond with the two active constraints at A' and the last term to the collinearity condition which also applies at A'. Similarly, point C' is determined by setting $v_1(\mathbf{u}, w) = v_1^{max}$, $v_2(\mathbf{u}, w) = v_2^{min}$ and $u_2 = (u_1 + 1)\tan(w)$. In both cases the optimization code *LFOPCV3* [40] reduces the error value to zero, giving the desired solutions.

A comparison between the workspace boundaries obtained and depicted here, with the results of Haug et al. [12], shows that equally accurate results are obtained with relative ease using the basic optimization approach.

2.6.3.2 Curves Connecting Bifurcation Points

From further inspection of Figure 2.9 and Figure 2.10, it is apparent that in the standard case only six, and in the modified case only five of the eight bifurcation points occur on the boundary. The remaining two points for the standard case are $G(1\ 1\ 0)$ and $H(0\ 0\ 1)$, and occur in the interior. For the modified case point $B(1\ 0\ 1)$ is also an interior point. These interior bifurcation points, at which in each case three constraints are active, may be determined in exactly the same manner as previously described for the boundary bifurcation points. For the standard case bifurcation points G and H almost coincide in the **u** plane. The precise respective coordinates are:

$$\text{for } G(1\ 1\ 0),\ u_1 = 0.92857151,\ u_2 = 1.3608971,\ w = -0.38025119$$

$$\text{and for } H\ (0\ 0\ 1), u_1 = 0.93166249,\ u_2 = 1.363325,\ w = 0.37183426$$

These results are exactly the same as those given by Haug et al. [12].

To complete the picture, interior curves connecting boundary bifurcation points to interior bifurcation points, and along which only one of the actuator lengths is allowed to vary, were also computed. These interior curves are of importance since, according to Haug et al. [42], limits on controllability of the planar Stewart platform are associated with configurations lying on the interior curves.

The method of mapping the interior curves is described with reference to the representative curve connecting boundary bifurcation point $A(1\ 1\ 1)$ to $G(1\ 1\ 0)$. Along this curve $[1\ 1\ -]$, $v_1 = v_1^{max}$, $v_2 = v_2^{max}$ and v_3 varies between v_3^{max} and v_3^{min}. M points along this curve may be mapped by successively solving, for $j = 1,2,3,...,M$, the following set of non-linear equations:

$$\begin{aligned} v_1(\mathbf{u}, w) - v_1^{max} &= 0 \\ v_2(\mathbf{u}, w) - v_2^{max} &= 0 \\ v_3(\mathbf{u}, w) - v_3^{j} &= 0 \end{aligned} \qquad (2.25)$$

$$\text{where } v_3^{j} = v_3^{max} - \frac{j}{M}\left(v_3^{max} - v_3^{min}\right)$$

This may readily be done by minimizing the sum of the squares of the residual errors, again using the *LFOPCV3* optimization code. For clarity, the computed interior curves are shown separately on Figure 2.11 and Figure 2.12 for the two individual platforms.

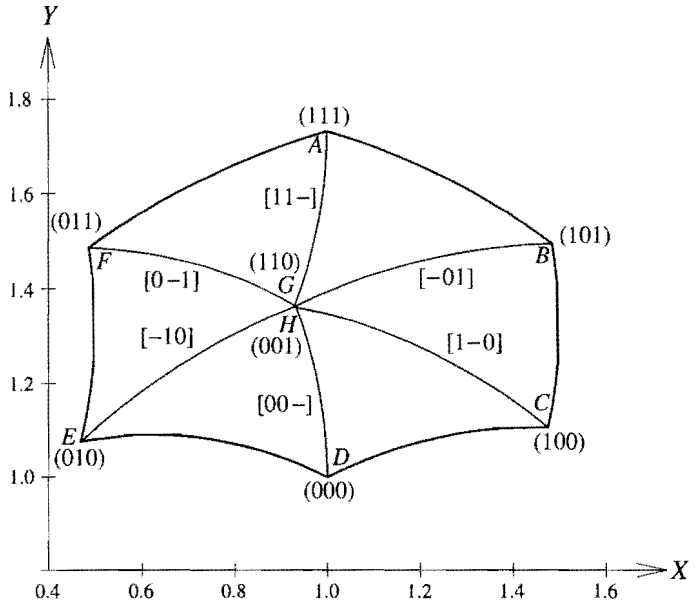

Figure 2.11 Computed curves for the *standard* planar Stewart platform ($1 \le l_3 \le \sqrt{3}$).

A final matter of interest concerns paths FH $[0\ -\ 1]$ and HD $[0\ 0\ -]$ for the *modified* planar Stewart platform shown in Figure 2.12. Along each of these paths there are respective points F' and D' at which, with leg 1 at its minimum position, a collinear and singular configuration is assumed. These points F' and D' are computed in a manner similar to the determination of A' and C' described in Section 2.6.3.1, but now with $v_1 = v_1^{\min}$. The circular arc $F'D'$, of radius $1+\sqrt{2}$ and center at global coordinates $(x, y) = (-1, 0)$, therefore designates the path of the working point when the planar Stewart platform assumes a collinear configuration with actuator leg 1 at its minimum position.

This concludes the presentation of the accessible workspace results for the planar Stewart platform. From an implementation point of view, it is important to state that all the techniques described here, and used to generate the workspace boundary and bifurcation curves, are integrated in a *Fortran* computer code *PLANSTEW* that is easy to use. The user specifies the limits on the leg lengths, and the code then automatically computes and plots the accessible workspace boundaries, as well as the curves connecting the bifurcation points situated on the outer boundary with those situated inside the accessible output set. The code *PLANSTEW* is available from the author on request. The details of the code is explained in Appendix A.

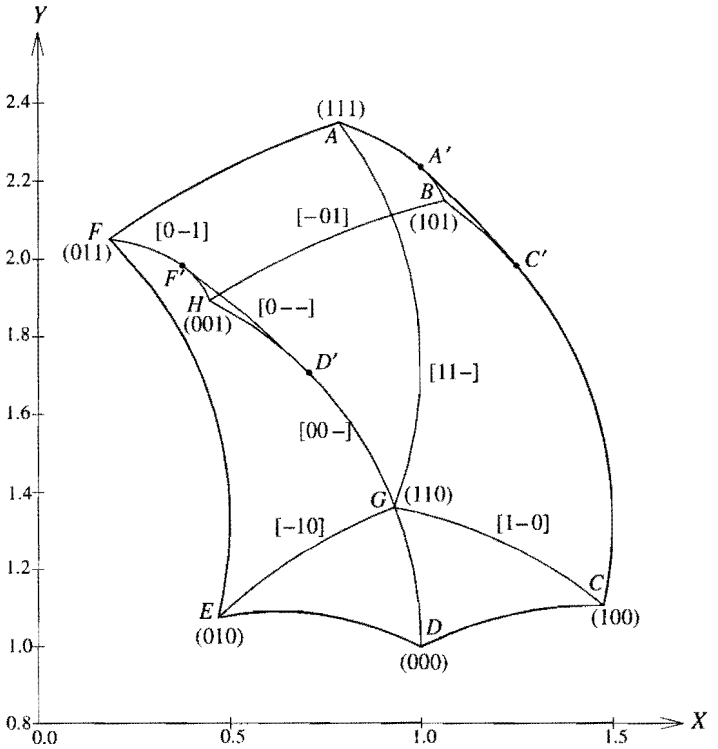

Figure 2.12 Computed curves for the *modified* planar Stewart platform ($1 \leq l_3 \leq 3$).

Note that nothing has been said about the values that the orientation angle φ assumes within the workspace. While determining the boundaries of the *accessible* workspace, the main interest is the maximum allowable displacement from the radiating point $\mathbf{u}^0$ irrespective of orientation. The value of the orientation angle φ is only a concern if it is apparent that the top platform assumes a flipped configuration where interference of the legs with each other becomes a possibility.

The next section deals with determining the *dexterous workspace* of the planar Stewart platform, where the orientation angle plays a primary role.

2.6.4 Determining the Dexterous Workspace of the Planar Stewart Platform

2.6.4.1 Introduction

The *dextrous workspace* of a parallel manipulator is *defined* by Haug et al. [8] as: "(the boundary of) the set of points that can be reached by a given point on the working body and at which specified *ranges* of rotation of the working body can be achieved." Clearly the dextrous workspace is not unique but depends on the specified ranges of rotations. It is also apparent that for any non-zero range of orientations the dextrous workspace will be a subset of the accessible workspace.

Haug et al. [8] explain that it is important to distinguish between the dexterous workspace and the accessible workspace of a manipulator. The literature often discusses the "workspace" of a manipulator, yet it often happens that the manipulator cannot "work" while following a continuous path within this so called workspace [43, 44], because it is essentially an accessible rather than a dextrous workspace and contains points at which no range of rotation is possible.

From the definition of a dextrous workspace it follows that for any given manipulator, a range of dextrous workspaces exists. Once the dexterity requirements for the manipulator are stipulated, the dexterous workspace within which the specific dexterity requirements are satisfied, can be determined. Adjusting the dexterity requirements will obviously result in a completely different dextrous workspace.

Haug et al. [8] mention that dexterity requirements for a manipulator are often stated in terms of ranges of mobility, normally rotatability, that must be achieved at each point in the desired accessible output set.

For the planar Stewart platform under consideration, any range of rotatability will be specified with relation to the orientation angle φ of the top platform, i.e. φ must be able to assume *all* values in the range $[\varphi_{min} - \varphi_{max}]$ at *any* point in the associated dextrous workspace.

With the orientation angle φ of the planar Stewart platform defined as the intermediate coordinate w ($w = \varphi$, see Section 2.6.2), one may naïvely expect that any such dexterity requirement can directly be translated to inequality constraints imposed on the intermediate coordinate of the form.

$$w_{min} \leq w \leq w_{max} \tag{2.26}$$

Seeing that expression (2.26) corresponds to expression (2.3), it is possible to solve optimization *Problem (i)* with the additional inequalities as given by expression (2.26). With reference to Section 2.3 this would imply maximizing the displacement from the radiating point $\mathbf{u}^0$ with inequality constraints imposed in both the actuator leg lengths (input coordinates) and the orientation angle of the top platform (intermediate coordinate).

The optimum solution to this problem (maximum displacement from $\mathbf{u}^0$) does however not yield points at the boundary where *all* orientations in the range $[\varphi_{min} - \varphi_{max}]$ are possible. In fact in general one may expect only one possible orientation in the range at a specific boundary point, and therefore the boundary thus obtained will not coincide with the boundary of the dextrous workspace for $[\varphi_{min} - \varphi_{max}]$.

In order to compute the dextrous workspace for the range $[\varphi_{min} - \varphi_{max}]$, denoted by $\boldsymbol{A}[\varphi_{min} - \varphi_{max}]$, it is necessary to first consider the fixed orientation accessible workspace $\boldsymbol{A}[\varphi_{fix}]$.

2.6.4.2 The Fixed Orientation Accessible Workspace of the Planar Stewart Platform

Consider the situation where a single dexterity requirement needs to be defined for the planar Stewart platform. This is the case where the accessible workspace for a fixed orientation of the moving platform is to be determined. Such a *fixed orientation* requirement is expressed as an equality:

$$\varphi = \varphi_{fixed} \tag{2.27}$$

and the associated accessible workspace is denoted by $\boldsymbol{A}[\varphi_{fix}]$.

Equation (2.27) is in actual fact an equality constraint fixing the value of the intermediate coordinate, i.e.

$$w = w_{fixed} \tag{2.28}$$

If, instead of the additional inequality constraints (2.26), an additional equality constraint (2.28) is added to optimization *Problem (i)*, the optimum solution will correspond to a position where the *fixed orientation* requirement is achieved. The *modified* optimization *Problem (i)* is:

***Modified* Problem (i)**:

$$\underset{\mathbf{u},w}{\text{maximize}} \ \left\|\mathbf{u} - \mathbf{u}^0\right\|$$

$$\text{such that:} \quad \mathbf{v}^{min} \le \mathbf{v}(\mathbf{u}, w) \le \mathbf{v}^{max}$$

$$\text{and subject to equality constraints:} \quad \begin{matrix} \mathbf{h}(\mathbf{u},\mathbf{s}) = \mathbf{0}, \ \mathbf{h} \in \mathrm{R}^{nu-1} \\ w = w_{fix} \end{matrix}$$

Solving the modified problem yields a point on the boundary of the fixed orientation accessible workspace. The complete boundary of $\boldsymbol{A}[\varphi_{fix}]$ may now be numerically mapped as before, by solving the modified problem for successive rays emanating from $\mathbf{u}^0$ at angular intervals δ (see Figure 2.2).

2.6.4.3 Computed Fixed Orientation Accessible Workspaces of the Planar Stewart Platform

The fixed orientation workspace $\boldsymbol{A}[0^\circ]$ where the top platform is fixed in a horizontal orientation, i.e., $\varphi = \varphi_{fixed} = 0^\circ$, is shown in Figure 2.13. The angular unrestricted accessible workspace is shown for

comparison purposes. The fixed orientation workspace is clearly a proper subset of the accessible workspace.

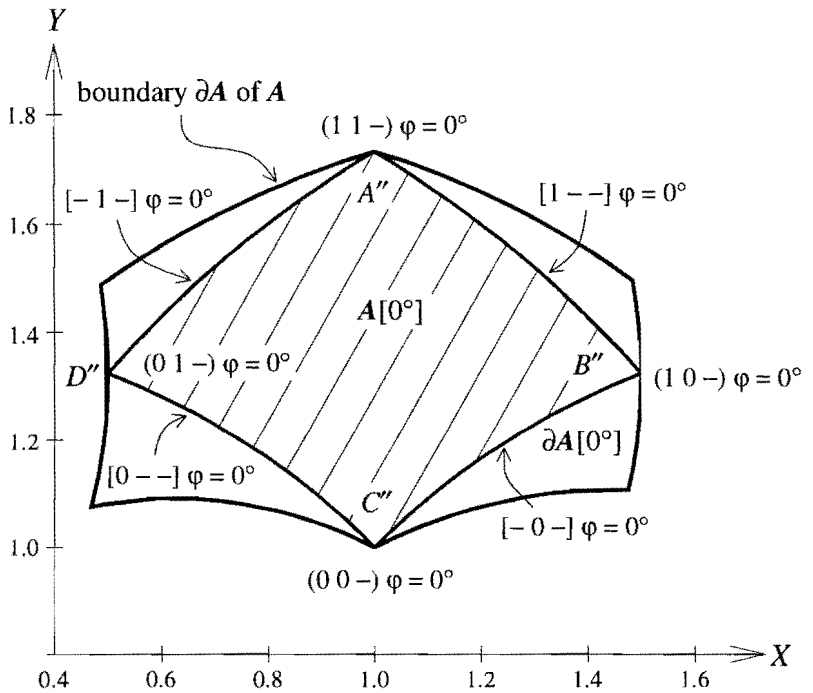

Figure 2.13 Fixed orientation workspace $A[0^\circ]$ inside the unrestricted accessible workspace A.

As an extension to the proposed labeling notation (see Sections 2.5.3 and 2.6.3), the bifurcation points and boundary curves of the fixed orientation accessible output set $A[0^\circ]$ are also labeled. Here the labeling notation is slightly modified to include the specification of the fixed orientation $\varphi = 0^\circ$.

The mapping of each of the four boundary curves is characterized by the active "search direction" equality constraint, the active "fixed orientation" equality constraint and also a single active inequality constraint. This means that only one actuator leg is at an extreme length as the working point advances along the fixed orientation boundary curves shown in Figure 2.13.

Each of the four bifurcation points therefore correspond to the position of the working point with at least two legs at extreme lengths. Consider for example bifurcation point B'', which is labeled $(1\ \ 0\ \ -)\ \varphi = 0^\circ$. This label indicates that for the dexterity requirement $\varphi = 0^\circ$, the working point coincides with bifurcation point B'' if $l_1 = l_1^{\max}$ and $l_2 = l_2^{\min}$. The length of actuator leg 3 is determined by the fixed orientation $\varphi = 0^\circ$.

As a result of the choice of leg length limits, the top platform is horizontal when it is in its highest possible and lowest possible positions. This is why bifurcation points $A''(1\ \ 1\ \ -)\ \varphi = 0^\circ$ and

$C''(0\ \ 0\ \ -)\ \varphi = 0^\circ$ in Figure 2.13 respectively coincide with bifurcation points $A(1\ \ 1\ \ 1)$ and $C(0\ \ 0\ \ 0)$ in Figure 2.9. The choice of the actuator leg length limits allows labeling bifurcation points A'' and C'' as: $A''(1\ \ 1\ \ 1)\ \varphi = 0^\circ$ and $C''(0\ \ 0\ \ 0)\ \varphi = 0^\circ$.

The fixed orientation boundary curves are labeled in a similar manner. Boundary curve $A''B''$ is, for example, labeled $[1\ \ -\ \ -]\ \varphi = 0^\circ$ showing that $l_1 = l_1^{max}$ as the working point advances along this curve. Actuator leg 2 varies from its minimum length at bifurcation point B'' to its maximum length at bifurcation point A'', and once again, l_3 is determined by the fixed orientation $\varphi = 0^\circ$. The other bifurcation points and boundary curves are similarly labeled (see Figure 2.13).

2.6.4.4 Using Fixed Orientation Workspaces to Determine a Dextrous Workspace

The mapping of the fixed orientation workspace may now be extended to determine the dextrous workspace $A[\varphi_{min} - \varphi_{max}]$ where the dexterity requirement is:

φ to assume *all* values in the range $[\varphi_{min} - \varphi_{max}]$ at *any* point in the dextrous workspace (2.29)

It should be clear that $A[\varphi_{min} - \varphi_{max}]$ is given by the intersection of all possible $A[\varphi_{fix}]$, $\varphi_{fix} \in [\varphi_{min} - \varphi_{max}]$. Since it is expected that $A[\varphi_{fix}]$ varies in a "continuous" manner with φ_{fix}, the reasonable assumption is now made that $A[\varphi_{min} - \varphi_{max}]$ may be obtained by simply considering the intersection of the extreme fixed angle sets, i.e.

$$A[\varphi_{min} - \varphi_{max}] = A[\varphi_{min}] \bigcap A[\varphi_{max}] \tag{2.30}$$

The validity of assumption (2.30) may in practice be reinforced by checking whether at the intermediate central value, φ_i, the following condition is satisfied:

$$\{A[\varphi_{min}] \bigcap A[\varphi_{max}]\} \subset A[\varphi_i] \tag{2.31}$$

where $\varphi_i = (\varphi_{min} + \varphi_{max})/2$.

{Indeed for the examples considered here condition (2.31) is more than satisfied – see Figure 2.13 where $A[\varphi_i] = A[0^\circ]$.}

Thus, if the orientation of the top platform is fixed to the minimum value as specified in the fixed orientation requirement, i.e. $\varphi = \varphi_{fixed} = \varphi_{min}$, the minimum fixed orientation workspace $A[\varphi_{min}]$ is mapped. Next the maximum fixed orientation ($\varphi = \varphi_{fixed} = \varphi_{max}$) set $A[\varphi_{max}]$ is mapped. The intersection or overlapping area is the dextrous workspace $A[\varphi_{min} - \varphi_{max}]$ within which the full dexterity requirement (2.29) is met.

2.6.4.5 Computed Dextrous Workspace

As an example of the application of the above methodology, consider the following rotatability requirement for the top platform of the planar Stewart platform:

$$\varphi \text{ to assume } \textit{all} \text{ values in range } [(-10^\circ)-(10^\circ)] \text{ at } \textit{any} \text{ point in } \boldsymbol{A}[(-10^\circ)-(10^\circ)]$$

The minimum fixed orientation workspace $\boldsymbol{A}[-10^\circ]$ and maximum fixed orientation workspace $\boldsymbol{A}[10^\circ]$ are shown in Figure 2.14. The intersection or overlap of these two workspaces gives the dextrous workspace $\boldsymbol{A}[(-10^\circ)-(10^\circ)]$, indicated by the shaded region, within which the full range rotatability is achieved.

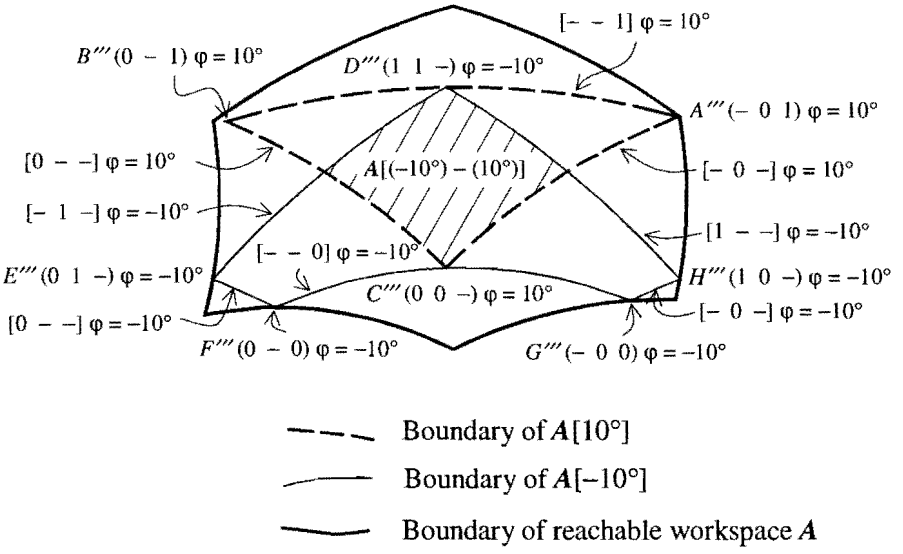

Figure 2.14 Dextrous accessible output set $\boldsymbol{A}[(-10^\circ)-(10^\circ)]$.

In accordance with the work of Haug et al. [8], the boundaries of the dexterous accessible output sets for which φ achieves the full ranges $[(-5^\circ)-(5^\circ)]$, $[(-10^\circ)-(10^\circ)]$ and $[(-15^\circ)-(15^\circ)]$ of rotatability are respectively shown in Figure 2.15. These boundaries are plotted together with the boundaries of the fixed orientation workspace $\boldsymbol{A}[0^\circ]$ and of the orientationally unrestricted workspace $\boldsymbol{A}$.

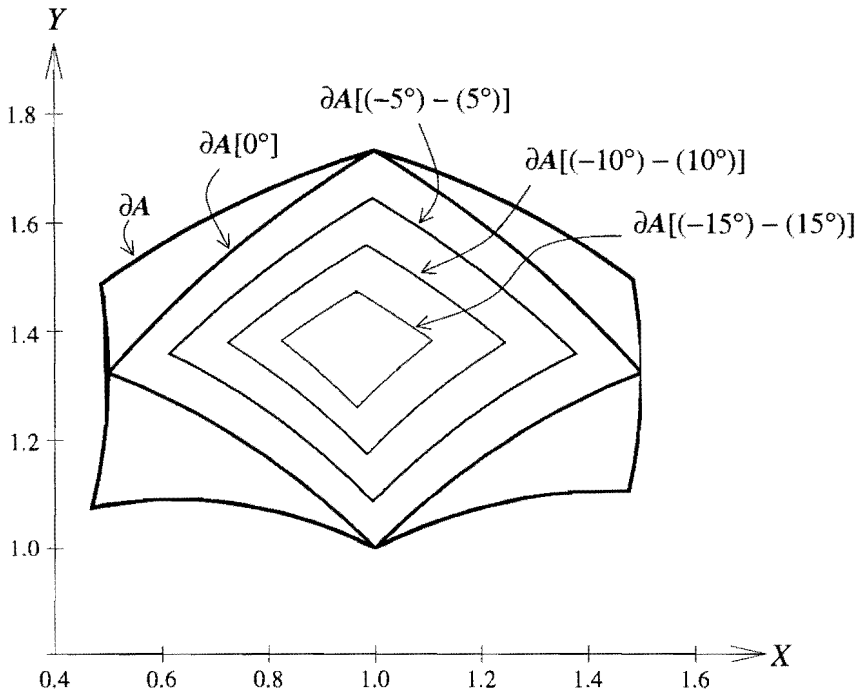

Figure 2.15 Dextrous accessible output sets for different full-range rotatability requirements.

Figure 2.15 correspond exactly to the results obtained by Haug et al. [8], and when analyzed, the results confirm the accuracy of the method proposed here.

The orientationally unrestricted accessible workspace is, as expected, bounded by the exterior boundary ∂A shown in Figure 2.15. For each search direction, the top platform is "displaced" further and further away the radiating point $\mathbf{u}^0$, as far as the leg length limits allow. It follows that for each point along the boundary of the reachable workspace, the orientation of the top platform depends on the extreme lengths of the two "active" actuator legs of that search direction.

As soon as the orientation of the top platform is fixed the maximum displacement from $\mathbf{u}^0$ is limited by the first actuator leg reaching its extreme length. This explains why the fixed orientation workspaces $A[\varphi_{fix}]$ are smaller than the unrestricted accessible workspace. Forcing the orientation of the top platform to remain fixed, prohibits any further rotation of the top platform. With no orientation limits imposed, the top platform can be tilted differently for each search direction, allowing for a maximum displacement from $\mathbf{u}^0$ which corresponds to an orientation with more than one actuator leg reaching its extreme value.

2.7 CONCLUSION

The optimization approach presented in this chapter successfully determines the workspaces of the planar manipulators investigated here. It is evident that this new optimization approach represents a very promising general tool for determining *and* analyzing manipulator workspaces. Computing the boundary of the workspace using the optimization approach allows the various sections of the workspace boundary, to be related to the behavior of the manipulator.

A new and concise notation for labeling the different bifurcation points and curves is also introduced here. It is believed that this, in general, greatly facilitates the description of the behavior of mechanisms within and on the boundary of the associated workspaces.

The computer code *PLANSTEW* demonstrates the ability to automate the process to allow the user to automatically map both outer boundaries of the accessible output sets and interior curves. The interior curves represent configurations at which controllability or mobility of the manipulator may be limited.

As far as the dextrous workspace is concerned, the approach proposed by Haug et al. [8] can successfully account for full range rotatability requirements of closed loop manipulators. However, one of the concluding remarks of Haug et al. is: "...the computations that result in solving the necessary conditions of the boundaries of the accessible output sets, however are shown to be tedious even for the planar manipulators studied". In contrast, the approach presented here may easily be implemented and automated.

The optimization approach also accounts for the full range rotatability requirements, and because the dexterity requirement is simply treated as an additional equality constraint, the dextrous accessible output set is easily mapped.

In the next chapter, the optimization approach, as developed here for planar manipulators, is extended to apply to a six-legged spatial Stewart platform.